ISSN 1995-0780, Nanotechnologies in Russia, 2019, Vol. 14, Nos. 5–6, pp. 204–215. © Pleiades Publishing, Ltd., 2019.
Russian Text © The Author(s), 2019, published in Rossiiskie Nanotekhnologii, 2019, Vol. 14, Nos. 5–6.

FUNCTIONAL AND CONSTRUCTION NANOMATERIALS

Stabilized Titanium Dioxide Nanoparticles: Preparation and Physicochemical, Photocatalytic, and Antimicrobial Properties

L. V. Safyanova[a,*], O. I. Timaeva[a,], G. M. Kuzmicheva[a,***], N. A. Lobanova[a,****], R. G. Chumakov[b,*****], E. V. Khramov[b,******], R. P. Terekhova[c,*******], and N. V. Sadovskaya[d,********]**

[a] *Russian Technological University MIREA, Moscow, 119571 Russia*
[b] *"Kurchatov Institute" National Research Center, Moscow, 123182 Russia*
[c] *Vishnevsky Institute of Surgery, Russian Ministry of Health, Moscow, 115093 Russia*
[d] *Karpov Institute of Physical Chemistry, Moscow, 105064 Russia*
**e-mail: lidiyasaf@mail.ru*
***e-mail: gertrudejames@mail.ru*
****e-mail: galina_kuzmicheva@list.ru*
*****e-mail: lavanda20002000@yandex.ru*
******e-mail: Chumakov_rg@rrcki.ru*
*******e-mail: evxramov@gmail.com*
********e-mail: terekhova@ixv.ru*
*********e-mail: nataly_sadovska@mail.ru*

Received July 5, 2019; revised July 5, 2019; accepted September 16, 2019

Abstract—The anatase nanoparticles are stabilized with titanium tetraisopropoxide $Ti[OCH(CH_3)_2]_4$ and isopropyl alcohol without surfactants suitable for biological studies. We showed that the hydrodynamic radii in suspensions depend on temperature and the duration of hydrolysis, whereas the composition (a mixture of anatase with brookite, anatase, brookite, and rutile) and the sizes of crystallites (X-ray), nanoparticles, and aggregates (SEM) in the dried state are mainly dependent on the pH of the environment. The nonphase of the samples stems from coherent intergrowth of unit cells of anatase and brookite via geometric and structural complementarity. We found that photocatalytic activity (PCA; Rhodamine 6G model dye under UV radiation) depends on OH/H_2O ratio (adsorbed), whereas antimicrobial activity (AMA) in the dark depends on an amount of free water on the surface of nanoparticles according to X-ray photoelectron spectroscopy (XPS). We revealed that samples with the smallest sizes of nanoparticles of all levels possess the highest PCA and AMA relative to *Staphylococcus aureus* and *Escherichia coli*.

DOI: 10.1134/S199507801903011X

INTRODUCTION

The nanosized titanium(IV) oxides are promising objects for scientific studies and practical applications due to their photocatalytic, catalytic, optical, bactericidal properties, etc., which depend on size effects [1]. These effects appear when the size of nanoparticles is <100 nm, and significant differences arise when the particle sizes are less than 30 nm. There is a specific size range for a specific property: ~2–30 nm for magnetic nanoparticles [2], ~30–60 nm for optical properties, [3], ~10–25 nm for photocatalysis, ~1–10 nm for catalysis [4–6], ~4–5 nm for biology [7], and ~3–10 nm for nanomedicine [8]. Moreover, the optimal properties depend on the modification of nanoscale titanium oxide(IV) [9].

The disperse systems are thermodynamically unstable: the processes leading to a decrease in free surface energy and, as a result, to an increase in particle size proceed at the interface. The degree of aggregation depends on synthesis conditions (temperature, duration, and pH of environment), and variation makes it possible to obtain nanosized titanium(IV) oxides in different phase states: anatase, brookite, or rutile [10]. Nanoparticles are stabilized either via formation of a double electric layer on their surface through the introduction of low molecular weight electrolytes into the sol (electrostatic mechanism) or via adsorption of low molecular weight surfactants or polymer stabilizers on the particle surface (steric mechanism) [11].

Table 1. Preparation conditions for suspensions

Sample	Hydrolysis temperature, °C	Hydrolysis time, h	pH
1	80	6	<1
2	80	4	
3	22	6	1.2
4	50	6	
5	80	1	<1
6	80	8	

The aim of this work is the stabilization of titanium dioxide nanoparticles without the participation of surfactants and their description.

EXPERIMENTAL

Synthesis. The nanosized titanium dioxide samples were prepared by mixing titanium tetraisopropoxide $Ti[OCH(CH_3)_2]_4$ (Sigma Aldrich) with isopropyl alcohol in a 6:1 volume ratio. The mixture was added dropwise to an aqueous solution of nitric acid HNO_3 (700 mL/L) during constant stirring, and the resulting sol was kept at different temperatures (22–80°C) for different hydrolysis times (1–8 h), then cooled to room temperature (Table 1).

The resulting suspensions were dried in an oven at 40(±2)°C to obtain powder samples.

Dynamic light scattering (DLS). The hydrodynamic diameter of TiO_2 particles in the suspension was found with a DLS on a Malvern Zetasizer Nano-ZS photon particle analyzer (Great Britain). Measurements were taken with thermostatically controllable cuvettes; the range of particle measuring was 0.6–6000 nm, with operation temperature at 2–120°C and detection angle of scattered light at 173°, and the light source was a helium-neon laser with λ = 633 nm at 4 mW. The results were processed with Malvern instruments software.

X-ray acquisition of the powder samples was performed *on an HZG-4 diffractometer* (graphite monochromator and CuK_α radiation in a step-by-step mode: pulse acquisition time was 10 s, step size was 0.02°, and angle interval 2θ = 2–80°). The "Program for processing diffraction patterns with the adjusting of initial data" [12] was used in this work. The average sizes of TiO_2 crystallite were assessed according to $L = K\lambda/\beta\cos\theta$ (2θ ~ 25° for anatase, 2θ ~ 30° for brookite, and 2θ ~ 36° for rutile), where λ = 1.54051 Å and β was the integral peak width, with empirical coefficient K = 0.9. The standard deviation was ±5%. Qualitative analysis was performed with an ICDD PDF-4 database, whereas quantitative analysis of single-phase samples was performed according to the program [13] without taking into account the X-ray amorphous phase.

X-ray acquisition of the powder samples was carried out *with synchrotron radiation* (*SR*) at the STM experimental station of the Kurchatov SR source (Kurchatov Institute, Moscow) [14, 15]. Measurements were achieved during the transmission mode on a MAR CCD two-dimensional detector at λ = 0.68886 Å (*K*-edge of Zr), a distance of 20 mm from sample to the detector, and an exposure time of 20 min. Single crystal monochromators with a butterfly-type cut were used to scan energy: Si (220) for the *K*-edge of Ag and Si (111) for the L3 edge of Au.

X-ray photoelectron spectroscopy (XPS). The XPE spectra were acquired at the NANOFES station (Kurchatov Institute, Moscow) on a PHOIBOS 150 spectrometer (AlK_α radiation). The powder particles were deposited on the surface of an In foil (the vacuum in the spectrometer chamber was no more than 2×10^{-9} Torr during the acquisition of the spectra and the source power was 100 W). The spectra were acquired in the constant transmission energy regimen (120 eV for full-region spectra recorded with a step of 0.5 eV and for the spectra of individual lines with a step of 0.05 eV). The spectra were calibrated by peaks of Au $4f_{7/2}$ (83.8 eV) and Ag $3d_{5/2}$ (367.9 eV) for gold and silver, mounted on a holder.

Table 2. The hydrodynamic diameters *D* (in nm) of suspensions of samples 1–6 depending on particle distribution

Particle distribution	Sample											
	1		2		3		4		5		6	
	D, nm	%	*D*, nm	%	*D*, nm	%	*D*, nm	%	*D*, nm	%	*D*, nm	%
By intensity	48	98	46	100	98	100	85	85	19	100	52	100
	344	2					13	15				
	1											
By number	5.5	100	10	100	41	100	7	100	8.5	100	17	100
By volume	5	30	15	100	61	100	11	100	11	100	26	100
	14	70										

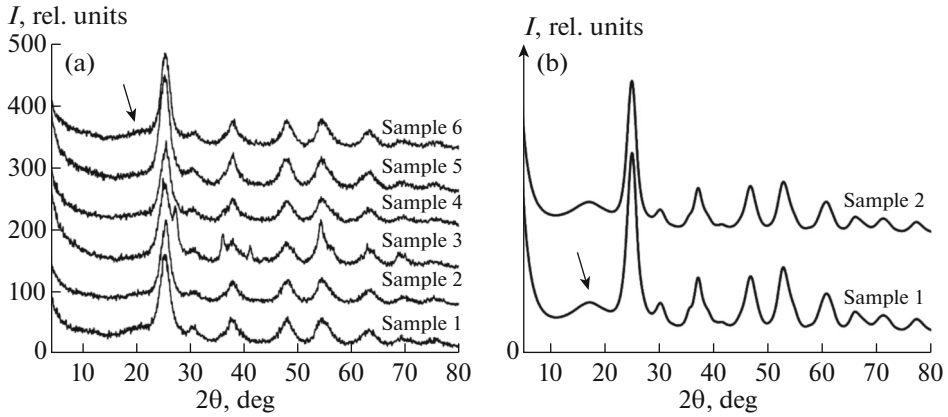

Fig. 1. Diffraction patterns of samples: (a) 1–6 (diffractometer) and (b) 1–2 (synchrotron).

The microstructure was studied with a *scanning electron microscopy (SEM)* on a high-resolution scanning electron microscope equipped with a JSM 7500F cold field emission cathode (JEOL, Japan) according to the procedure described in [16]. A program for the processing of electron microscopy images was used to analyze the images of microstructure with the construction of particle size distribution [17]. The elemental composition was found with X-ray spectral microanalysis (XSMA) on an INCA Penta FET-x3 energy dispersive microanalyzer (OXFORD INSTRUMENTS, United Kingdom). Areas with lateral sizes from 2 × 2 to 100 × 100 μm were studied. The analyzer was equipped with a nitrogen-cooled silicon-

Table 3. X-ray data of samples 1–6 (diffractometer)

hkl	Sample 1				Sample 2				Sample 3			
	85.5% of anatase + 14.5% of brookite				89.3% of anatase + 10.7% of brookite				85.5% of anatase + 6.8% of brookite + 7.7% of rutile			
	2θ, deg	*d*, Å	*I*, %	*L*, Å	2θ, deg	*d*, Å	*I*, %	*L*, Å	2θ, deg	*d*, Å	*I*, %	*L*, Å
	19.96*	4.445	21	25	20.25*	4.381	17	25				
101[1]	25.42	3.501	100	40	25.66	3.468	100	40	25.41	3.502	100	35
110[3]									27.41	3.251	27	70
121[2]	30.64	2.915	17	35	30.94	2.878	12	35	30.73	2.907	8	45
101[3]									36.2	2.479	9	115
004[1]	37.9	2.371	34	30	38.02	2.364	30	30	38.01	2.365	7	45
111[3]									41.28	2.185	5	110
200[1]	48.13	1.888	29	40	48.23	1.885	28	35	48.01	1.893	28	30
	Sample 4				Sample 5				Sample 6			
	87.0% of anatase + 13.0% of brookite				85.0% of anatase + 15.0% of brookite				90.9% of anatase + 9.1% of brookite			
	2θ, deg	*d*, Å	*I*, %	*L*, Å	2θ, deg	*d*, Å	*I*, %	*L*, Å	2θ, deg	*d*, Å	*I*, %	*L*, Å
									20.62*	4.304	13	20
101[1]	25.61	3.475	100	40	25.41	3.502	100	35	25.54	3.484	100	40
121[2]	30.61	2.918	15	35	30.63	2.916	18	30	30.97	2.885	10	45
004[1]	38.03	2.364	27	40	38.02	2.364	30	40	38.07	2.361	32	40
200[1]	48.11	1.889	29	35	47.99	1.894	28	30	48.06	1.891	35	35

[1] Anatase.
[2] Brookite.
[3] Rutile.
*$H_{0.572}Ti_{0.858}O_2$ (JCPDS 81-19).

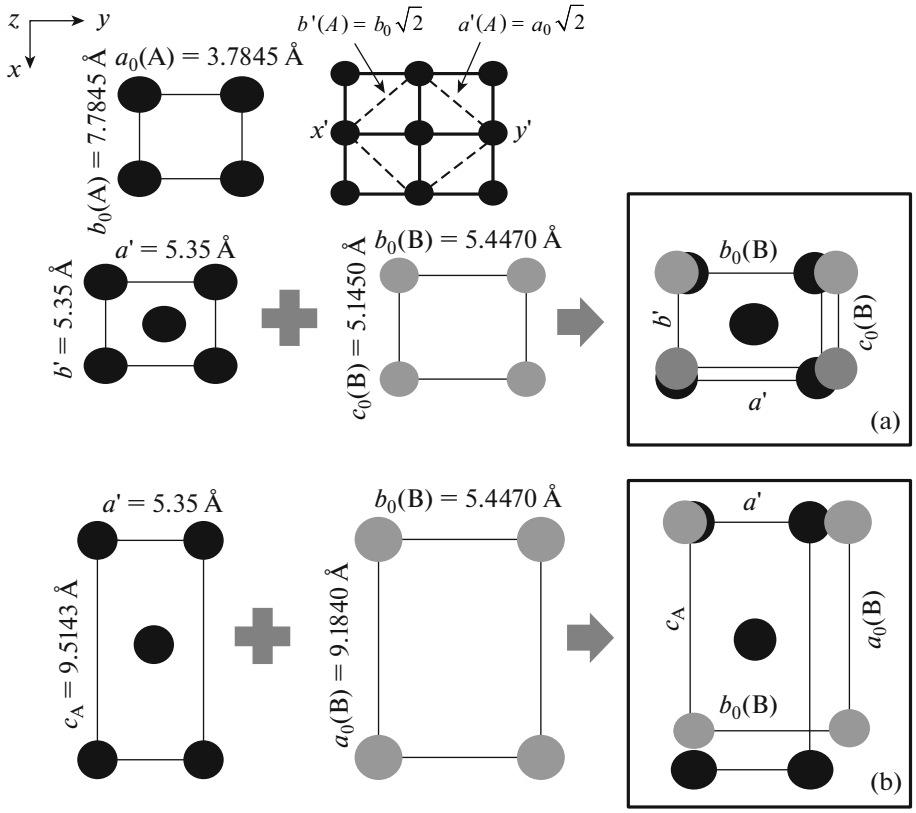

Fig. 2. The geometric correspondence of the following structures: (black) anatase and (gray) brookite. Coordinate axes: (a) XY and (b) XZ.

lithium detector; carbon resolution was 129 eV. The detector was calibrated with the CoK_α radiation of a reference cobalt metal. The elemental composition was measured at an electron probe energy of 15 keV, and depth λ, assessed with "The Depth of X-ray Production", was ~3.1 μm.

The photocatalytic activity (*PCA*) was assessed on model photocatalytic decomposition reactions of methyl orange (MeO) and rhodamine G dyes. The initial concentration of an aqueous dye solution (C_0) was 17 mg/L and the mass concentration of a suspended photocatalyst was 0.5 g/L. The ratio of a current dye concentration (after irradiating the mixture for 26 min with a 26 W UV mercury lamp) to the initial (C/C_0 value) was spectrophotometrically controlled through the change in intensity of an absorption band at a wavelength of ~490–510 nm for MeO and ~524 nm for Rhodamine G. The activities of different photocatalysts were compared from the reaction rate constant calculated graphically from the dependences. The rate constant (k) was calculated as a slope of a relationship between the substrate concentration C/C_0 and exposure time τ in rectifying semilogarithmic coordinates; the reliability of the linear approximation of the kinetic curves by the R factor in all cases was no lower than 0.95 and the error in determining the reaction rate constant was 5%.

The antimicrobial activity (*AMA*) was studied with the 'well' method for *Staphylococcus aureus*, *Escherichia coli*, and *Candida albicans* microorganisms. A microbial suspension of certain bacteria containing 10^7–10^8 CFU per 1 mL was inoculated with "lawn" into Petri dishes on a Mueller–Hinton agar at 0.2 mL. The holes, in which the test samples were placed, were made with a thin-walled cylinder at a diameter of 6–8 mm on the surface of agar seeded with microorganism cultures. The dishes were placed into a thermostat at 37°C for 24 h. The results were assessed from the size of a zone of growth inhibition of microorganisms around the hole; the diameter of microbial growth inhibition zones was found with a ruler, including that of the hole [18]. The degree of sensitivity of microorganisms to the samples depends on the size of their growth inhibition zone: the larger it is, the higher the sensitivity [19]. Microbiological studies were performed in a second-class microbiological protection box equipped with a UV lamp and a laminar airflow.

RESULTS AND DISCUSSION

Dynamic light scattering. Table 2 shows hydrodynamic diameters D (in nm) of nanoparticles in the suspensions depending on particle distribution.

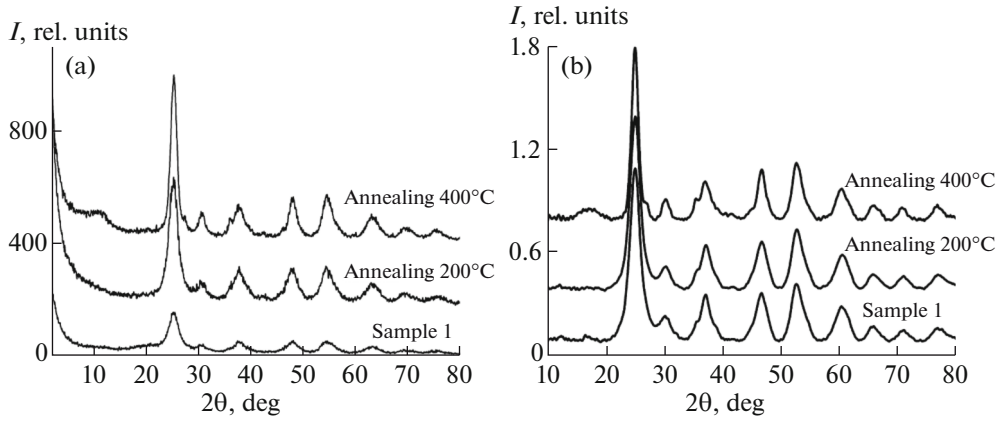

Fig. 3. Diffraction patterns of sample 1 and sample 1 annealed 1 h at 200°C and 400°C: (a) diffractometer and (b) synchrotron.

Almost all samples contain coarse (40–100 nm) and fine (5–20 nm) fractions in different proportions depending on a particle distribution. The D value is minimal for all distribution types for sample 5 (t = 80°C and τ = 1 h) (Table 2). All samples have the smallest hydrodynamic particle diameter D_{min} (in nm) with $D < 20$ nm, except sample 3.

We must understand the difference between the types of particle distribution and use them to correctly interpret DLS data. Heat capacity depends on volume or mass of a substance (distribution by volume), whereas the colligative properties of solutions and suspensions depend on number of particles per volume unit (distribution by number). The intensity distribution characterizes the properties of a suspension via light scattering. The distributions in number and volume are more important for practical purposes (for example, in biological studies) [20]. Considering these facts, the D_{min} value found from the number and volume is 5.5 (100%) and 5 nm (30%) for sample 1 (t = 80°C and τ = 6 h) (Table 2).

X-ray studies. X-ray diffraction data indicate that the powder samples are nonphase: they contain phases with an anatase structure (characteristic peaks at 2θ ~ 25, 38, 48, 55, 62, 70, and 75°; JCPDS 89-4921), brookite (2θ ~ 30°; JCPDS 75-1582) (samples 1, 2, 4, 5, and 6), and additionally rutile (2θ ~ 27, 36, and 41°; JCPDS 21-1276) (sample 3) (Fig. 1 and Table 3).

The diffuse halo at 2θ ~ 19° on the diffractograms of samples 1, 2, and 6, indicated with an arrow in

Table 4. X-ray data of sample 1 after heat treatment (diffractometer)

hkl	Sample 1				Sample 1 (annealing at 200°C)				Sample 1 (annealing at 400°C)			
	85.5% of anatase + 14.5% of brookite				87.0% of anatase + 10.4% of brookite + 2.6% of rutile				84.0% of anatase + 11.8% of brookite + 4.2% of rutile			
	2θ, deg	d, Å	I, %	D, Å	2θ, deg	d, Å	I, %	D, Å	2θ, deg	d, Å	I, %	D, Å
									11.04**	8.007	25	20
	19.96*	4.445	21	25								
101[1]	25.42	3.501	100	40	25.43	3.499	100	34	25.49	3.491	100	48
110[3]									27.56	3.233	5	79
121[2]	30.64	2.915	17	35	30.87	2.894	12	37	30.88	2.893	14	46
101[3]					36.09	2.486	3	90	36.26	2.475	5	87
004[1]	38.01	2.371	34	30	37.89	2.372	29	30	37.91	2.371	29	30
200[1]					48.01	1.893	27	33	48.11	1.889	33	38

[1]Anatase.
[2]Brookite.
[3]Rutile.
*$H_{0.572}Ti_{0.858}O_2$ (JCPDS 81-1949).
** $TiO_{2-x}(OH)_{2x} \cdot yH_2O$ (y ~ 1).

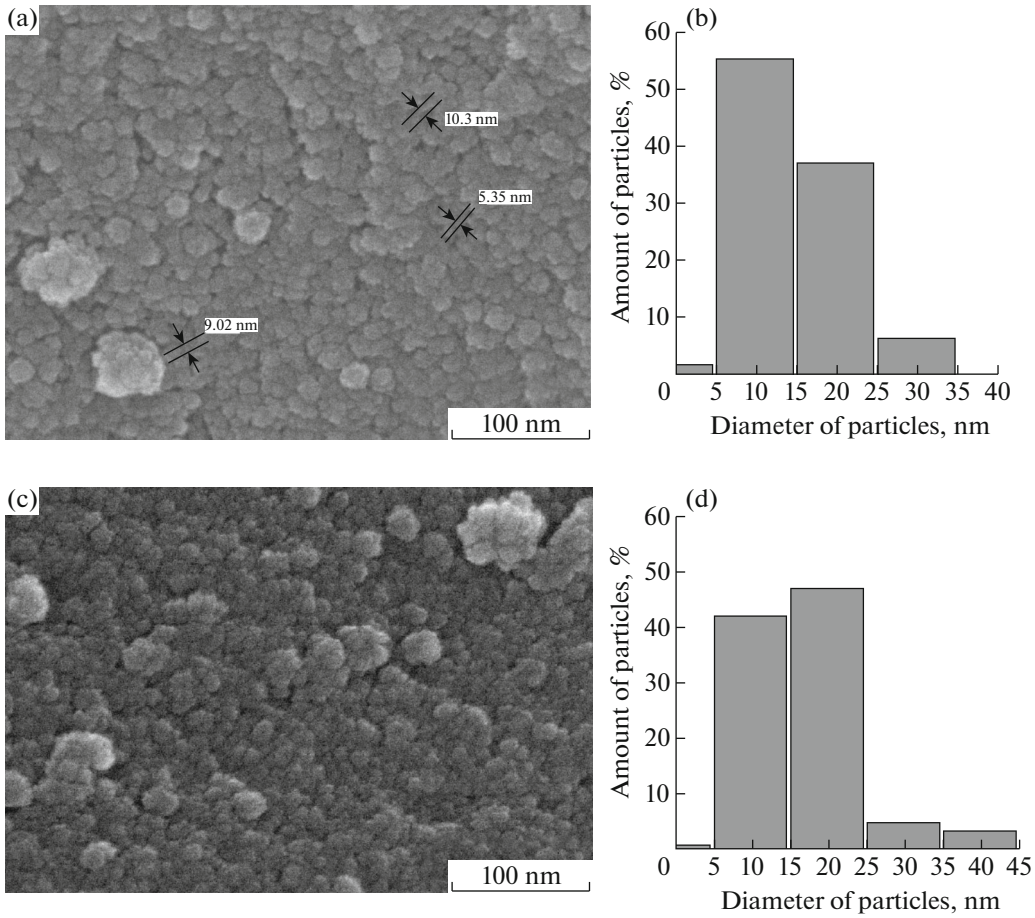

Fig. 4. Images of microstructure and particle size distribution of samples: (a, b) 1 and (c, d) 2.

Fig. 1 and marked with an asterisk in Table 3, is a result of the $H_{0.572}Ti_{0.858}O_2$ X-ray amorphous phase, from which composition is $H_2Ti_3O_{6.993}$ after transformation.

This composition is close to that of titanic acids of general formula $H_2Ti_xO_{2x+1}$ or $Ti_xO_{2x-1}(OH)_2$ with $x = 3$; brookite is formed, when $x = 3$ [21].

High sensitivity of SR makes possible to detect the impurity rutile phase in samples 1 and 2 in a small amount (peaks at $2\theta \sim 36$ and 41°) (Fig. 1b), whose peaks are much weaker on X-ray diffraction patterns.

The pH value of environment has a significant influence on the formation of nanosized titanium dioxide with different modifications: pH < 1 leads to a

Table 5. Elemental composition of the surface of the samples (at %) and peak positions (eV)

Elemental composition, at %	Peak position, eV		Sample 1	Sample 2	Sample 3	Sample 4	Sample 5	Sample 6
Ti	Ti–O	465 [25]	11.7	12.8	9.0	8.4	6.0	7.1
O	H_2O_1	535–537 [26]	33.8	34.6	21.6	22.1	12.1	25
	H_2O_2	538–540 [27]	3.6	2.3	–[3]	2.5	6.2	4.4
	OH	532–537 [28, 29]	18.4	21.5	14.8	23.1	19.0	11.6
	Ti–O	530 [30]	5.1	4.5	16.5	8.5	–[3]	–[3]
C	O–C=O	291 [31]	12.5	9.7	16.6	16.4	31.3	28.1
	N–C=O	287 [32]	8.8	8.1	9.7	7.1	2.5	1.4
	C–C	285 [32]	5.8	6.2	11.5	12.9	22.8	22.2

[1]Adsorbed H_2O.
[2]Free H_2O.
[3]There are no lines.

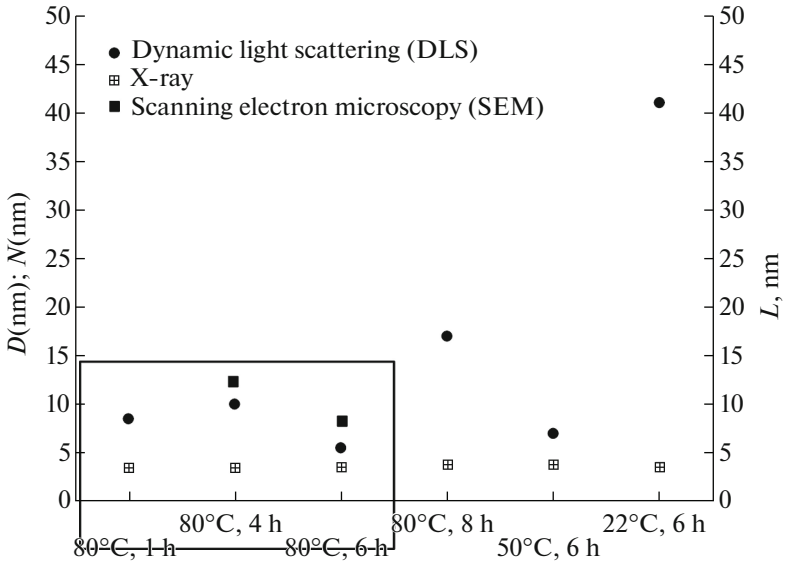

Fig. 5. The relationship between nanoparticle sizes found using three methods (where D is a hydrodynamic particle diameter (DLS method), L is average anatase crystallite size (X-ray), and N is nanoparticle size (SEM method)) and preparation conditions of samples.

brookite impurity metastable phase (samples 1, 2, 4, 5, and 6), whereas pH ~ 1.2 leads to a rutile stable modification (sample 3). The temperature and the duration of hydrolysis also influence the formation of a certain TiO_2 modification. In any case, the kinetic conditions of this synthetic process contribute to a rutile nanoscale phase at a much lower temperature than for a bulk sample; anatase and brookite are transformed into rutile at 800 and 750°C [22].

Anatase and brookite are in one sample because of their similar structural and geometric parameters. Figure 2 shows the coordinate planes of the anatase (A) (black in Fig. 2) with an $I4_1/amd$ space group and brookite (B) structures (gray in Fig. 2) with a *Pbca* space group.

The converted anatase unit cell parameters (a_0 = 3.7845 and c_0 = 9.5143 Å) in new perspective $a' = b' = a_0\sqrt{2}$ = 5.35 Å and parameters b = 5.4470 and c = 5.1450 Å in the XY plane of a brookite unit cell (a = 9.1840, b = 5.4470, and c = 5.1450 Å) in the YZ plane differ by ~ 4% (Fig. 2a). Parameters a' = 5.35 and c_0 = 9.5143 Å in the other XZ direction of anatase (A) cells differ from parameters b = 5.4470 and a = 9.1840 Å of brookite (B) cells in the XY plane, also by ~ 4% (Fig. 2b), so we may assume that they are coherently grown.

Table 6. Elemental composition (at %) of samples 1 and 2 according to RSMA

Element	Sample 1 (after five measurements)	Sample 2 (after six measurements)
Ti	45.55	38.00
O	35.81	52.09
C	18.64	9.91

The average crystallite size is different depending on modification of titanium dioxide: L = ~ 3.7 nm for anatase, ~3.75 nm for brookite, and ~11.0 nm for rutile (Table 3). These values are lower than that of nanosized anatase (L = ~ 4.0–5.0 nm) from titanyl sulfate as a precursor [23]. The other authors [24] also stabilized TiO_2 nanoparticles via hydrolysis of titanium tetraisopropoxide $Ti[OCH(CH_3)_2]_4$, however under different synthesis conditions (t = 70°C, τ = 7 h, and pH = 3.5 after the dialysis stage of sols). As a result, they obtained single-phase samples with anatase nanoparticles at L = 4.7 nm, within the range of nanoparticle values for the samples from the sulfate method [23].

Sample 1, having the smallest hydrodynamic diameter (according to DLS), was annealed at two temperatures, 200 and 400°C, for 1 h. Figure 3 shows the diffraction patterns of initial sample 1 and those annealed, and Table 4 shows X-ray data.

When temperature increases, there is an increase in the amount of rutile, a decrease in the amount of brookite in sample 1, and a slight increase in average crystallite size. Figure 3 shows that, when annealing temperature increases up to 400°C, a $TiO_{2-x}(OH)_{2x} \cdot yH_2O$ X-ray amorphous impurity phase with y ~1 appears in sample 1 (Table 4 and Fig. 3a), together with a diffraction peak at 2θ ~11–12° [21]. The acquisition of sample 1 on a synchrotron (Fig. 3b) leads to a different diffraction pattern of the same

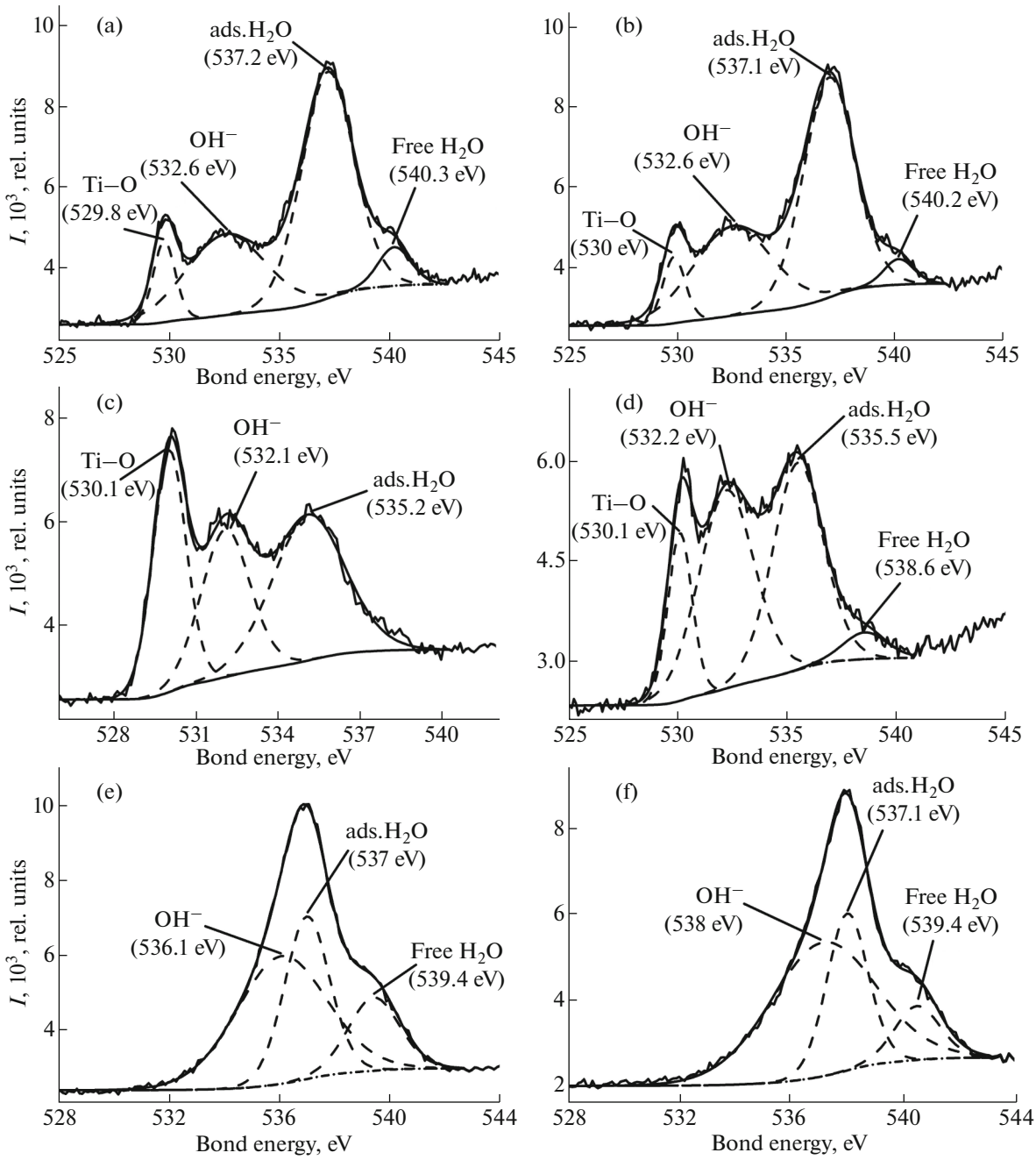

Fig. 6. O1*s* XPS spectra of samples: (a) 1, (b) 2, (c) 3, (d) 4, (e) 5, and (f) 6.

sample annealed at 400°C. A diffuse peak at ~20° indicates that there is a $H_{0.572}Ti_{0.858}O_2$ phase and not $TiO_{2-x}(OH)_{2x}\cdot yH_2O$ (Fig. 3a), via influence of SR on the sample. This should be taken into account during the acquisitions of nanoscale objects on a synchrotron.

SEM studies of samples 1 and 2 showed that they included small nanoparticles with a rather narrow distribution (Fig. 4). Sample 1, obtained via hydrolysis of $Ti[OCH(CH_3)_2]_4$ for 6 h, has a minimum nanoparticle size of $N = 10–15$ nm (Figs. 4a and 4b), whereas sample 2, prepared for a shorter hydrolysis time (4 h), has a slightly longer size, $N = 20$ nm (Figs. 4c and 4d). These samples also included associates with sizes of ~90 nm consisting of nanoparticles with $N = ~20$ nm (fractal formations). The $Ti[OCH(CH_3)_2]_4$ precursor, therefore, contributes to the preparation of small nanoparticles in the synthesis of titanium dioxide nanoparticles, since it enters easily into the hydrolysis reaction during contact with water to form OH groups, which act as a link between the resulting nanoparticles. In addition, isopropyl alcohol (a surfactant substitute)

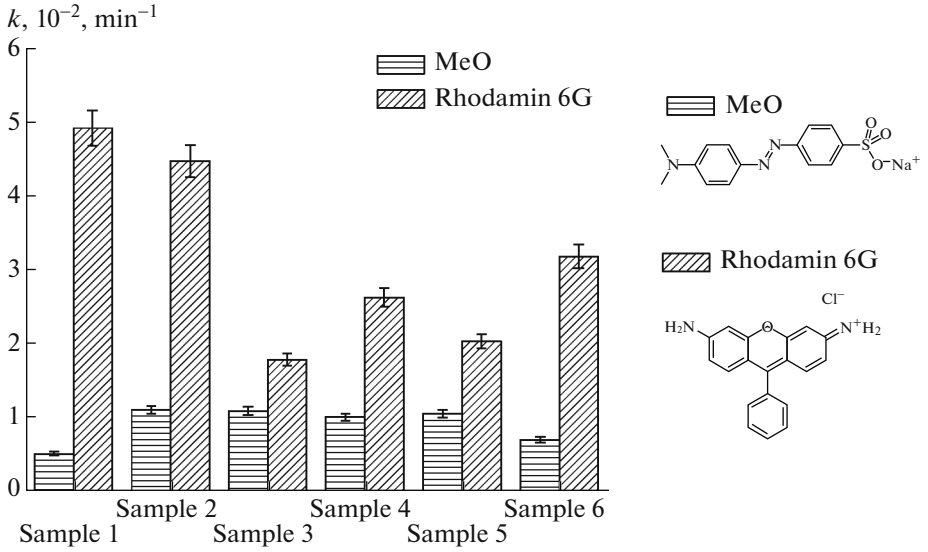

Fig. 7. Reaction rate constants k (in min^{-1}) of MeO and Rhodamine 6G dye photodegradation in the presence of samples 1–6.

provides the aggregative stability of particles in a suspension. Moreover, pH, temperature, and the duration of hydrolysis also have a significant effect in forming nanoparticles of different sizes.

Figure 5 shows the relationship between the conditions to obtain nanoparticles (temperature and duration of hydrolysis) and their sizes: D is a hydrodynamic particle diameter obtained via DLS method (in nm), L the average anatase crystallite size obtained via X-ray (in nm), and N is the nanoparticle size according to SEM data (in nm).

Samples 1 (t = 80°C and τ = 6 h), 2 (t = 80°C, τ = 4 h), and 5 (t = 80°C, τ = 1 h) are assigned to those with a minimum size of nanoparticles of all levels (Fig. 5). They contain the maximum amount of nanosized anatase.

X-ray photoelectron spectroscopy. Titanium, oxygen, and carbon are observed on the surface of nanoparticles of samples 1–6 (Fig. 6 and Table 5), i.e., those elements involved in titanium tetraisopropoxide $Ti[OCH(CH_3)_2]_4$, from which all samples were obtained.

The Ti2$p_{1/2}$ spectrum of all samples contains a band at ~ 465 eV assigned to Ti in Ti–O [25], and an amount of Ti–O in sample 2 is higher than that in others.

Three bands with bond energies of 285 eV (C in C–C), 287 eV (C in N–C=O), and ~ 291 eV (C in O–C=O) were found in the C1s spectra of samples 5, 3, and 6 with a maximum amount of 22.8, 9.7, and 28.1 at % (Table 5). The peaks at ~285 and ~291 eV are assigned to C=O and O–C=O and belong to carbon-containing surface contamination [31].

Samples 1 and 2 contain the largest amount of water (free and adsorbed) on their surface [26] (37.4 and 36.9 at %); moreover, sample 1 has more free water than that of sample 2 (Fig. 6 and Table 5). Samples 2 and 4 have the highest amount of O as OH groups compared with other samples (Fig. 6) [28, 29]: 21.5 and 23.1 at %.

X-ray microanalysis. Elemental analysis data indicate that the samples 1 and 2 contain titanium, oxygen, and carbon, which confirms the XPS results (Table 6).

Sample 2 has a higher amount of oxygen compared to that of sample 1, whereas sample 1 has a higher amount of carbon than that of sample 2 (Table 6), which is also in agreement with XPS data (Table 5).

The *photocatalytic activity* of samples 1–6 was assessed from the photodegradation reactions of an anionic methyl orange (MeO) and cationic Rhodamine 6G dyes (Rhodamine 6G) (Fig. 7).

The highest decomposition rate constants k_{max} (in min^{-1}) were observed for sample 1 (k_{max} ~ 0.0494 min^{-1}) and sample 2 (k_{max} ~ 0.0449 min^{-1}) (Rhodamine 6G) with the smallest particle sizes according to DLS data (with R_{min} at number = 5.5 nm (100%), R_{min} at volume = 5.0 nm (30%) and R_{min} at number = 10.0 nm (100%), R_{min} at volume = 15.0 nm (100%)) (Fig. 7 and Table 2). SEM data show that sample 1 has a nanoparticle size of 10–15 nm and sample 2 has a size of 20 nm (Fig. 3). The average sizes of anatase crystallites for samples 1 and 2 are L = ~4.0 nm (Table 3).

Higher PCA for the cationic Rhodamine 6G dye is due to greater adsorption on the surface of titanium dioxide nanoparticles caused by interaction with OH groups and H_2O adsorption molecules, which are larger in samples 1 and 2 according to XPS data (Fig. 4 and Table 5) in comparison with other samples (Fig. 8). In addition, OH groups, which interact with

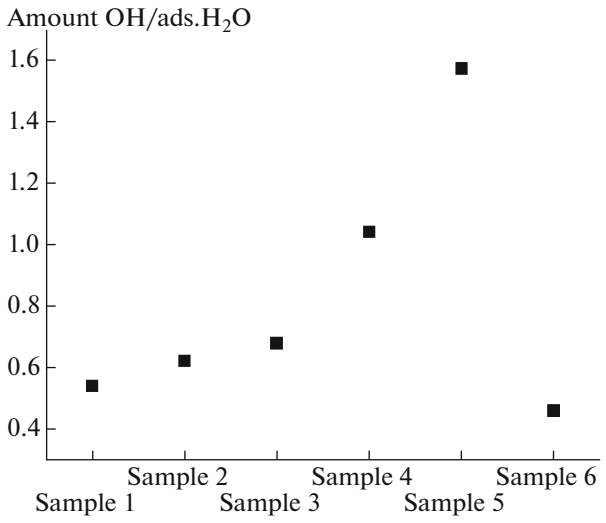

Fig. 8. Amount of OH groups/adsorbed H_2O ratio in samples 1–6 according to XPS data.

the cationic Rhodamine 6G dye, form Bronsted centers responsible for PCA.

Several characteristics that affect the PCA, therefore, may be distinguished: the composition of the samples (without rutile) (Table 3), the surface composition (the optimal ratio OH groups/H_2O adsorbed) (Fig. 8), and the minimum size of nanoparticles of all levels (Fig. 5).

Antimicrobial activity. The methodological recommendations imply [18] that the growth inhibition zone with a diameter of up to 10 mm indicates that there is no sensitivity, whereas 11–15 mm correspond to low sensitivity, 15–25 mm indicates that there is a sensitivity, and more than 25 mm correspond to high sensitivity of a microorganism to a drug. *Staphylococcus aureus* possesses high sensitivity to sample 5 according to this classification and, *Escherichia coli*, to sample 6. All samples have no antimicrobial activity against *Candida albicans* fungi (Fig. 9).

High AMA (Fig. 9) and the highest PCA (Fig. 7) are characteristic of different samples. Sample 5 has minimal hydrodynamic diameter *D* (in nm) according to all particle distributions (Table 2), the smallest sizes of its nanoparticles of all levels, as in samples 1 and 2, the highest amount of nanoscale anatase, the highest OH/adsorbed H_2O ratio (Fig. 8), and the highest amount of free water (Table 5). Water on the surface of nanoparticles provides penetration into a microorganism cell, so the water-ion transport of a cell is impaired, and the bacterial growth slows down or completely terminates [33, 34]. Sample 5 with the highest AMA against gram-positive *Staphylococcus aureus* and sample 6 with the highest AMA against gram-negative *Escherichia coli* (Fig. 8) contain a larger number of free water molecules on their surface (6.2 and 4.4 at %) compared with other samples. The structure of bacterial cell walls, however, cannot be ruled out. Gram-negative *Escherichia coli* is known to contain a thin and negatively charged outer lipopolysaccharide layer with 7–8 nm in thickness, whereas gram-positive *Staphylococcus aureus* consist of a thick and cross-linked solid peptidoglycan layer, 20–80 nm in thickness [35].

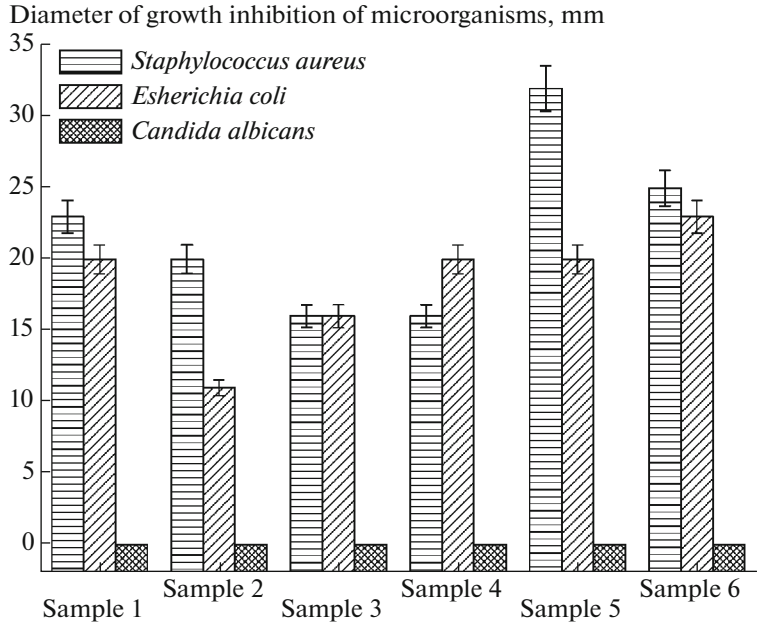

Fig. 9. Antimicrobial activity of the samples.

CONCLUSIONS

The stabilized anatase nanoparticles were obtained without surfactants, the best of which have sizes no more than 20 nm in suspensions and in the dried state, and contain a nanoscale brookite impurity. The photocatalytic and antimicrobial properties of the samples are due to different reasons, however samples with smaller nanoparticles are the most active. Samples with the highest photocatalytic activity in reaction to Rhodamine 6G (UV radiation) have low antimicrobial activity against *Staphylococcus aureus* and *Escherichia coli*, which is due to surface composition and different reactions to different types of water: PCA correlates with bound water and AMA does with the free.

FUNDING

This work was supported by the Russian Ministry of Education and Science (no. 4.1069.2017/PCh).

CONFLICT OF INTEREST

The authors declare that they have no conflict of interest.

REFERENCES

1. T. Moritz, J. Reiss, K. Diesner, et al., "Nanostructured crystalline TiO_2 through growth control and stabilization of intermediate structural building units," J. Phys. Chem. B **101**, 8052 (1997).
2. S. P. Gubin, Yu. A. Koksharov, G. B. Khomutov, and G. Yu. Yurkov, "Magnetic nanoparticles: preparation, structure and properties," Russ. Chem. Rev. **74**, 489 (2005).
3. A. N. Ignatov, *Optoelectronics and Nanophotonics* (Lan', St. Petersburg, 2011) [in Russian].
4. V. V. Sleptsov, I. I. Diesperova, A. A. Bizyukov, and S. N. Dmitriev, "Physicochemical aspects of formation of nanocomposite structures, Part II," Mikrosist. Tekh., No. 2, 28 (2002).
5. A. I. Gusev and A. A. Rempel', *Nanocrystalline Materials* (Fizmatlit, Moscow, 2001; Cambridge Int., Science Publ., Cambridge, 2004).
6. A. D. Pomogailo, A. S. Rozenberg, and I. E. Uflyand, *Nanoparticles of Metals in Polymers* (Khimiya, Moscow, 2000) [in Russian].
7. T. Paunesku, T. Rajh, G. Wiederrecht, et al., "Biology of TiO_2-oligonucleotide nanocomposites," Nat. Mater. **2** (5), 343 (2003).
8. I. S. Chekman, "Nanotechnology, nanomedicine, nanopharmacology, nanopharmacy: the introduction of results in medical practice," Probl. Endokrin. Patol., No. 1, 80 (2014).
9. G. M. Kuz'micheva, "Nanosized phases with titanium(IV) oxides. Preparation. Characterisation. Properties," Tonk. Khim. Tekhnol. **10** (6), 5 (2015).
10. Z. R. Ismagilov, L. T. Tsikoza, N. V. Shikina, et al., "Synthesis and stabilization of nano-sized titanium dioxide," Russ. Chem. Rev. **78**, 873 (2009).
11. I. S. Tyukova, A. P. Safronov, A. P. Kotel'nikova, and D. Yu. Agalakova, "Electrostatic and steric mechanisms of iron oxide nanoparticle sol stabilization by chitosan," Polym. Sci., Ser. A **56**, 498 (2014).
12. G. M. Kuz'micheva, V. V. Podbel'skii, A. N. Stepanov, and A. A. Gainanova, "Computer program for processing diffraction patterns of nanoscale and amorphous substances and calculation of the characteristics of the substructure," State Registration Certificate of Computer Program No. 2017610699.
13. G. M. Kuz'micheva, V. V. Podbel'skii, and A. A. Gainanova, "Program for qualitative and quantitative X-ray analysis of multiphase samples," State Registration Certificate of Computer Program No. 2016616402.
14. A. Chernyshov, A. Veligzhanin, and Y. Zubavichus, "Structural materials science end-station at the Kurchatov Synchrotron Radiation Source: recent instrumentation upgrades and experimental results," Nucl. Instrum. Methods Phys. Res., Sect. A **603**, 95 (2009).
15. N. Trofimova, A. Veligzhanin, V. Murzin, et al., "Structural diagnostics of functional nanomaterials with the use of X-ray synchrotron radiation," Ross. Nanotechnol. **8**, 396 (2013).
16. L. N. Obolenskaya, G. M. Kuz'micheva, E. V. Savinkina, N. A. Prokudina, V. V. Chernyshov, and N. V. Sadovskaya, "Effect of sulfate synthesis conditions on characteristics of samples with the nanosized η-TiO_2 modification," Russ. J. Inorg. Chem. **57**, 1177 (2012).
17. G. M. Kuz'micheva, V. V. Podbel'skii, O. I. Timaeva, and L. R. Iskhakova, "Program for processing IR spectra and correlation of absorption bands with standards," State Registration Certificate of Computer Program No. 2017611789.
18. B. M. Datsenko, S. V. Biryukova, and T. I. Tamm, *Guidelines for the Experimental (Preclinical) Study of Drugs for Local Treatment of Purulent Wounds* (MZ SSSR Farmakol. Komitet, Moscow, 1989) [in Russian].
19. L. A. Blatun, "Baneotsin (powder, ointment)—perspective for use in complex surgical treatment of purulonecrotic diseases of the lower extremities in patients with diabetic foot syndrome," Rany Ranev. Infekts., Zh. Kostyuchenka **2** (3), 36 (2015).
20. V. E. Eskin, *Light Scattering by Polymer Solutions and the Properties of Macromolecules* (Nauka, Leningrad, 1986) [in Russian].
21. M. Dadachov, "Novel titanium dioxide, process of making and method of using same," US Patent No. 2006/0171877.
22. S. K. Filatov, V. S. Grunin, M. V. Razumeenko, and T. V. Alekseeva, *Crystal Chemistry and X-ray Diffraction of Minerals* (Nauka, Leningrad, 1987) [in Russian].
23. A. A. Gainanova, G. M. Kuz'micheva, and I. G. Vasil'eva, "Nanosized low-temperature phases of titanium(IV) oxide with anatase and η-phase structures: composition, structure, and photocatalytic properties," Russ. Chem. Bull. **67**, 1350 (2018).
24. Z. R. Ismagilov, N. V. Shikina, N. A. Mazurkova, et al., "Synthesis of nanoscale TiO_2 and study of the effect of their crystal structure on single cell response," Sci. World J. **498345**, 1 (2012).

25. J. Choi, J. Song, K. Jung, et al., "Bipolar resistance switching characteristics in a thin Ti–Ni–O compound film," Nanotecnology **20** (17), 1 (2009).
26. L. Q. Wang, D. R. Baer, M. H. Engelhard, and A. N. Shultzc, "The adsorption of liquid and vapor water on TiO_2 (110) surfaces: the role of defects," Surf. Sci. **344**, 237 (1995).
27. D. Liitzenkirchen-Hecht and H. H. Strehblow, "Bromide adsorption on silver in alkaline solution: a surface analytical study," Ber. Bunsen-Ges. Phys. Chem. **6**, 826 (1998).
28. G. M. Kuz'micheva, E. V. Savinkina, L. N. Obolenskaya, L. I. Belogorokhova, B. N. Mavrin, M. G. Chernobrovkin, and A. I. Belogorokhov, "Synthesis, characterization, and properties of nanoscale titanium dioxide modifications with anatase and η-TiO_2 structures," Crystallogr. Rep. **55**, 866 (2010).
29. A. Suganys, G. Shanmugavelayutham, and C. S. Rodriguez, "Study on plasma pre-functionalized PVC film grafted with TiO_2/PVP to improve blood compatible and antibacterial properties," J. Phys. D: Appl. Phys. **50**, 1 (2017).
30. A. Abidov, B. Allabergenov, J. Lee, et al., "X-ray photoelectron spectroscopy characterization of Fe doped TiO_2 photocatalyst," Int. J. Mater. Mech. Manuf. **1**, 294 (2013).
31. J. F. Moulder, W. F. Stickle, P. E. Sobol, and K. D. Bomben, *Handbook of X-Ray Photoelectron Spectroscopy,* Ed. by J. Chastain (Perkin Elmer, MN, 1992), Vol. 40.
32. H. J. Kim, I. S. Bae, S. J. Cho, et al., "Synthesis and characteristics of NH_2-functionalized polymer films to align and immobilize DNA molecules," Nanoscale Res. Lett. **7**, 1 (2012).
33. M. A. Radtsig, "Interaction of bacterial cells with silver and gold compounds: effects on growth, biofilm formation, mechanisms of action, biogenesis of nanoparticles," Cand. Sci. (Biol.) Dissertation (Lomonosov Mosc. State Univ., Moscow, 2013).
34. E. V. Bessudnova, "Synthesis and study of nanosized particles of titanium dioxide for use in catalysis and nanobiotechnology," Cand. Sci. (Biol.) Dissertation (Boreskov Inst. Cata. Sib. Branch of RAS, Novosibirsk, 2014).
35. M. Qasim, N. Udomluck, J. Chang, H. Park, and K. Kim, "Antimicrobial activity of silver nanoparticles encapsulated in poly-N-isopropylacrylamide-based polymeric nanoparticles," Int. J. Nanomed. **13**, 235 (2018).

Translated by A. Tulyabaev